Nonlinear Treatment of a Black Hole Mimicker Ringdown

Nils Siemonsen*
Princeton Gravity Initiative, Princeton University, Princeton, New Jersey 08544, USA
and Department of Physics, Princeton University, Princeton, New Jersey 08544, USA

(Received 1 May 2024; accepted 24 June 2024; published 19 July 2024)

We perform the first nonlinear and self-consistent study of the merger and ringdown of a black hole mimicking object with stable light rings. To that end, we numerically solve the full Einstein-Klein-Gordon equations governing the head-on collisions of a series of binary boson stars in the large-mass-ratio regime resulting in spinning horizonless remnants with stable light rings. We broadly confirm the appearance of features in the extracted gravitational waveforms expected based on perturbative methods: the signal from the prompt response of the remnants approaches that of a Kerr black hole in the large-compactness limit, and the subsequent emissions contain periodically appearing bursts akin to so-called gravitational wave echoes. However, these bursts occur at high frequencies and are sourced by perturbations of the remnant's internal degrees of freedom. Furthermore, the emitted waveforms also contain a large-amplitude and long-lived component comparable in frequency to black hole quasinormal modes. We further characterize the emissions, obtain basic scaling relations of relevant timescales, and compute the energy emitted in gravitational waves.

DOI: 10.1103/PhysRevLett.133.031401

Introduction—The black hole is a remarkably successful paradigm explaining astrophysical observations driven by highly compact and dark objects. Despite this success, a large class of alternative objects has been developed [1], challenging this paradigm. These objects—black hole mimickers—are horizonless and imitate many or all of the observable signatures of black holes. Cardoso *et al.* pointed out that the light ring structure around these objects plays a central role in the ringdown of any black hole mimicker [2–4]. They observed that the gravitational wave (GW) emissions promptly after an extreme-mass-ratio merger of a binary black hole mimicker is universally identical to that of a black hole ringdown, independently of the mimicker's internal structure. The emitted signal deviates from the black hole ringdown only after a light-crossing time of the interior of the mimicker and is characterized by repeated burstlike GW echoes. As argued in Refs. [2–4], the prompt response can be understood as the partial reflection of the GWs sourced by the plunging companion off of the unstable light ring of the primary black hole mimicker. The subsequent echoes are due to repeated leakage of the transmitted gravitational perturbations traversing across the stable light ring in the mimicker's interior.

As a mechanism to discover as of yet unknown new physics, the ringdown of black hole mimickers has received much attention. Broadly, efforts have been devoted to understanding the ringdown of various classes of black hole mimickers [2,3,5–17], computing waveforms and templates [18–28], determining detection prospects with GW detectors [29–32], and searching for burstlike emissions in the GW data following known binary coalescence events [33–44] (see Ref. [45] for a review). Despite the immense progress of this program, results were largely obtained modeling the internal structure of the mimicker by boundary conditions a small distance away from the would-be horizon and treating it's dynamical response at the test-field and extreme-mass-ratio level. Thereby neglecting, (i) nonlinear gravitational effects, (ii) coupling of the mimicker's internal structure to gravitational degrees of freedom even at the linear level, (iii) self-interactions of the matter making up the object, and (iv) any finite size effects of the objects. Notably, a few approaches have been developed in Refs. [46–49] to address some of these shortcomings. However, a fully nonlinear and self-consistent treatment of the merger and ringdown of a black hole mimicker is still lacking. This leaves many important questions unanswered. In particular, when including all effects (i)–(iv), are the prompt emissions indeed identical to those of a ringing black hole? What are the amplitudes of the quasinormal modes of the remnant excited during the merger? Specifically, is the waveform following the prompt ringdown solely characterized by GW echoes? How does the remnant's spin impact these conclusions?

In this work, we address these questions fully self-consistently in the large-mass-ratio and head-on merger setting. To that end, we drop all restrictions (i)–(iv) by performing a series of four fully nonlinear numerical time-domain evolutions of coalescing spinning binary boson stars—a particular set of black hole mimickers—resulting in spinning horizonless remnants with stable light rings. We

*nils.siemonsen@princeton.edu

find that the prompt dynamical response of the remnants, encoded in the emitted GWs, approaches that of Kerr black holes in the large-compactness limit. The subsequent emissions contain both a high-frequency burstlike component with frequency set the binary's size ratio, and a large-amplitude and long-lived component indicative of excited trapped modes in the remnant's interiors.

Model and methods—Boson stars [50,51] are the most developed highly compact and black hole mimicking objects that can be treated within numerical relativity [52,53]. Those stars relevant for this work are solutions in the theory with Lagrangian [54]

$$\mathcal{L} = \frac{R}{16\pi} - g^{\mu\nu}\partial_{(\mu}\bar{\Phi}\partial_{\nu)}\Phi - \mu^2|\Phi|^2\left(1 - \frac{2|\Phi|^2}{\sigma^2}\right)^2, \quad (1)$$

where $g_{\mu\nu}$ is the metric with Ricci scalar R, and Φ is the complex scalar field making up the star with mass parameter μ and self-interaction strength σ. Here and in the following, we employ $G = c = 1$ units. Boson stars are characterized by a harmonic dependence on both coordinate time t and azimuthal coordinate φ, i.e., $\Phi \propto e^{i(\tilde{\omega}t + \tilde{m}\varphi)}$, set by their internal frequency $\tilde{\omega}$ and index $\tilde{m}$. Therefore, spinning stars (with $|\tilde{m}| > 0$) exhibit toroidal surfaces of constant scalar field magnitude. So far, no binary boson star evolution has resulted in remnants with stable light rings [3,55–67]. We proceed by focusing entirely on spinning stars [68–70] with $\tilde{m} = 3$ and $\sigma = 0.035$. Stars in models with strong scalar self-interactions, e.g., $\sigma \ll 1$, as well as with larger $\tilde{m}$, exhibit larger compactnesses. The sequence of four binary boson stars considered in this work have mass ratios $q = M/M_*$ and size ratio $\eta = R/R_*$ between the primary (heavier) star of mass M and radius R and the secondary (lighter) binary constituent of mass M_* and radius R_*. We define $M_0 \approx M$ to be the Arnowitt–Deser–Misner mass of the binaries for later convenience. In all cases, the primary exhibits large compactness $C = M/R$; the secondary is the same $C_* = 0.02$ star in all cases. The properties of the binaries are summarized in Table I. Isolated star solutions are used to generate constraint-satisfying binary initial data as described in Refs. [64,71]. All primary stars, and due to the large mass-ratio all merger remnants, exhibit a pair of counter-rotating stable and unstable light rings. We focus solely on large mass-ratio systems, as the merger remnant of a comparable mass-ratio binary is likely a black hole (for further details see the Supplemental Material [72]). In what follows, we identify the binaries by the compactness of the primary constituent. We also evolve a single black hole–boson star collision, where we replaced the $C = 0.38$ primary star by a black hole of the same mass and spin. The initial coordinate separation is $D/M_0 = 160$ and the objects are boosted to Newtonian freefall velocities from infinity. Since the numerical evolutions are performed imposing axisymmetry on the metric and azimuthal symmetry $\partial_\varphi\Phi = 3i\Phi$ on the scalar field, a nonaxisymmetric instability [71,97] likely present in these stars is (artificially) quenched; see the Supplemental Material for further details.

TABLE I. Properties of the primary boson star in the sequence of binaries. The secondary with frequency $\tilde{\omega}_*/\mu = 0.85$, mass $M_*\mu = 0.24$, and angular momentum $J_*/M_*^2 = 12.1$, is the same in all binaries considered. The last two columns show the mass and size ratios q and η of the binaries, respectively.

C	$\tilde{\omega}/\mu$	J/M^2	$M\mu$	q	η
0.38	0.105	0.95	18.7	78	4.4
0.36	0.111	0.98	17.5	73	4.3
0.32	0.130	1.08	13.9	58	3.9
0.28	0.150	1.22	11.0	46	3.5

Results—Our first main result is that the prompt dynamical response of the merger remnant encoded in the emitted GWs approaches the response of a Kerr black hole towards large compactnesses. In Fig. 1, we show the waveforms emitted during the plunge and merger of the sequence of binaries and compare these with the aforementioned black hole–boson star binary. While there are differences in amplitude in the $\ell = 2$, 3 modes, the frequencies of all $\ell = 2$, 3, 4 modes broadly match with the black hole response, and scale, analogous to black

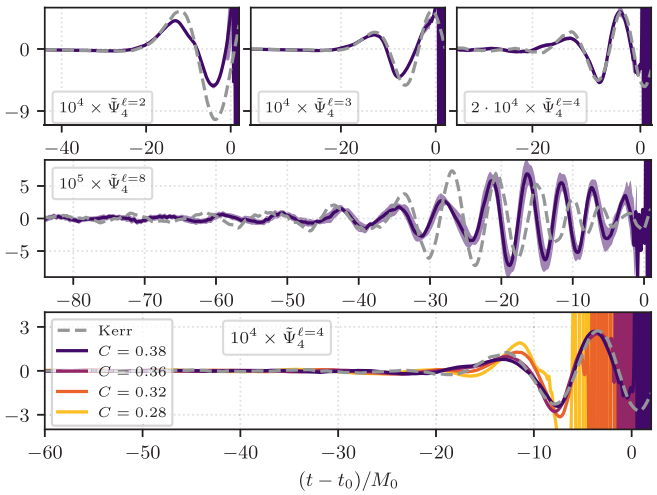

FIG. 1. The GWs emitted during the merger of the binaries labeled by their primary star compactness compared to the black hole–boson star binary labeled "Kerr" (top and center panels contain the $C = 0.38$ and Kerr binaries only). We show the ℓth spin-weighted spherical harmonic component of the Newman-Penrose scalar $\tilde{\Psi}_4^\ell = r_{\rm extr} M_0 \Psi_4^\ell$ extracted on spheres of coordinate radius $r_{\rm extr}/M_0 = 100$ and with coordinate time t. All waveforms are time shifted by aligning at the largest peak of the $\ell = 2$ mode, whereas t_0 corresponds to the transition time from prompt to subsequent emissions of the $C = 0.38$ binary. The colored band indicates uncertainties of our methods.

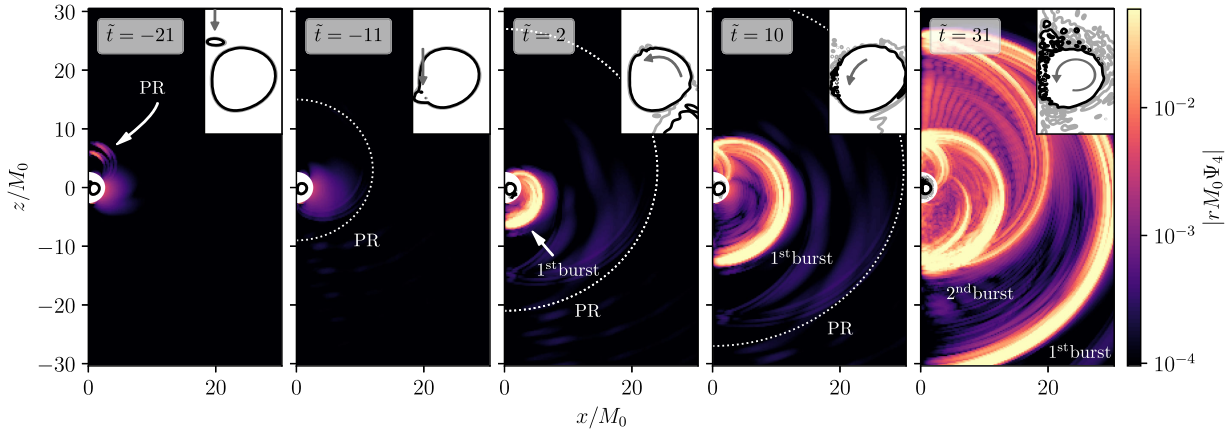

FIG. 2. The state of the $C = 0.38$ binary system at selected coordinate times $\tilde{t} = (t - t_0 + r_{\rm extr})/M_0$ during the plunge, merger, and ringdown. The main plots show the Newman-Penrose scalar Ψ_4 at coordinate radii $r > 3M_0$, which qualitatively shows the local GWs. We indicate the initial production and subsequent propagation of the high-frequency component of the prompt response as "PR" together with a dotted white circle (roughly corresponding to the propagating wavefronts). Similarly, the first two GW bursts are labeled 1st and 2nd. In the region $r < 3M_0$, we show two (black and gray) surfaces of constant scalar field magnitude $|\Phi|$ (with a close-up in the insets); recall, spinning boson stars are toroidally shaped. Arrows in the insets indicate the motion of the largest perturbation of $|\Phi|$ between snapshots. The symmetry axis is at $x = 0$.

hole quasinormal modes, (roughly) linearly with ℓ. Since $C = 0.38$ is still a relatively low remnant compactness, the peaks of the $\ell = 2, 3, 4$ "Kerr" waveforms are buried in the subsequent emissions. However, we find higher-ℓ modes to peak earlier leading to a separation of the prompt response and subsequent emissions. Fitting for these $\ell = 8$ frequencies and decay rates of the $C = 0.38$ and Kerr cases (shown in Fig. 1), we find that the former differ by $\approx 15\%$, while the latter are consistent to within the uncertainties of our methods (though, the peak times differ by $\approx 5M_0$). We discuss these differences below. Lastly, in the bottom panel of Fig. 1, we present the $\ell = 4$ waveforms for all four binaries. From there we conclude that the more compact the remnant (i.e., the longer the interior's light crossing time) the more and longer it's response is black-hole-like. All in all, our nonlinear and self-consistent treatment of the large-mass-ratio problem broadly confirms expectations based on perturbative calculations.

To understand the system's dynamics during the plunge and merger, we present snapshots of the evolution of the $C = 0.38$ case in Fig. 2. Around $\tilde{t} \approx -25$ (the high-ℓ part of) the prompt Kerr response is produced as the secondary approaches the primary [98] (first panel). While the latter propagates outwards, the binary merges and well-localized perturbations propagate along the symmetry axis through the remnant's interior (second panel). As these perturbations reach the opposing side and begin propagating poloidially around the remnant's outer edge, the first gravitational (and scalar) wave burst is emitted (third panel). Before the second burst is emitted, the perturbations propagate through the interior along the symmetry axis a second time as indicated by the gray arrows (fourth panel). The perturbations come around a third time in the last panel. At this stage, the perturbations dispersed into a collection of gravitationally bound states around the remnant (see the last panel of Fig. 2). As a point of comparison, the light crossing time of null geodesics in the $C = 0.38$ isolated solution traveling along the axis from $z = M/C$ to $z = -M/C$ as seen by distant observers is $\tau_{\rm axis}/M = 19.6$.

Turning now to the gravitational waveform emitted after the prompt response. Our second main result is that these emissions exhibit bursts akin to GW echoes reappearing after roughly a light-crossing time through the remnant's interior and with frequency set by the secondary's size. In Fig. 3, we present the $\ell = 2$ and $\ell = 8$ gravitational waveforms after the prompt emissions. Both modes contain a set of high-frequency bursts of frequency $f_{\rm burst}$ and separated by a timescale $\tau_{\rm burst}$. The burst's frequency can be understood as follows: The spatial scale $R_* \approx M_0/(\eta C)$ of the secondary object sets the length scale λ of the perturbations sourced within the remnants interior: $\lambda \lesssim R_*$. In Fig. 4, we identify these perturbations as the source of the bursts, by finding good agreement between the underlying length scales, i.e., $f_{\rm burst}^{-1} \lesssim R_*$, for all four binaries considered. From the central panels of Fig. 3, we see that in contrast to the black hole ringdown frequencies, the burst frequency is independent of the polar mode number ℓ. The burst period $\tau_{\rm burst}$ is less straightforward to understand. At the test-field level, high-frequency gravitational perturbations sourced by the merger are propagating roughly along null geodesics. Therefore, most naturally the burst period is compared to the light crossing time of null geodesics traversing the remnant's interior along the direction of the perturbations sourced during the merger, i.e., $\tau_{\rm axis}$, as defined above. In Fig. 4, we compare $\tau_{\rm burst}$ against this light crossing time $\tau_{\rm axis}$, again finding good agreement

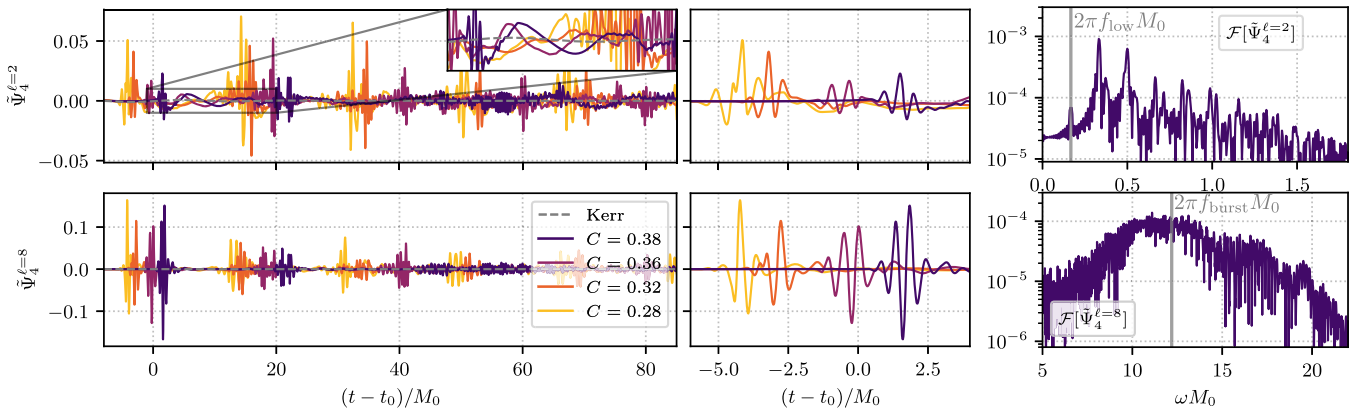

FIG. 3. (left panels) The $\ell = 2$ (top) and $\ell = 8$ (bottom) components of the GWs emitted after the merger of the sequence of four binary boson stars compared with that of the black hole–boson star binary (labeled Kerr); t_0 divides the prompt response and first burst of the $C = 0.38$ binary, is defined as in Fig. 1. (central panels) Close-ups of the first bursts in each of the two polar modes. (right panels) The Fourier transform of the full $C = 0.38$ signal as function of angular frequency ω, focusing only on dominant radiation components in each mode: the long-lived component in the $\ell = 2$ mode (top) and the burstlike high-frequency component in the $\ell = 8$ mode (bottom); we indicate $f_{\rm low}$ and $f_{\rm burst}$. See the Supplemental Material for details on uncertainties of these waveforms.

$\tau_{\rm burst} \approx \tau_{\rm axis}$. However, $\tau_{\rm axis}$ is to be understood only as a rough measure of crossing times, since purely considering null geodesics to determine the burst period neglects that during the merger massless (gravitational) and massive (scalar) modes are coupled and the relevant dynamics are not confined only to the axis. Overall, the appearance of burstlike emission components separated by a light crossing time of the remnants interior is consistent with the expectations based on test-field calculations. On the other hand, the burst's frequency $f_{\rm burst} \gtrsim \mathcal{O}(1)M_0 > f^{\rm Kerr}_{\ell m=20}$, at the considered size ratios, is much larger than the corresponding black hole quasinormal mode frequencies [99,100], and hence, larger than test-field computations predict the GW echo frequency, and decay rates, to be [15,18,20]; this is further discussed below.

Our third main result is that the low-multipole GW emissions contain a large-amplitude and long-lived component. As evident from Fig. 3 (close-up of the top left panel and Fourier transform in the top right panel), the

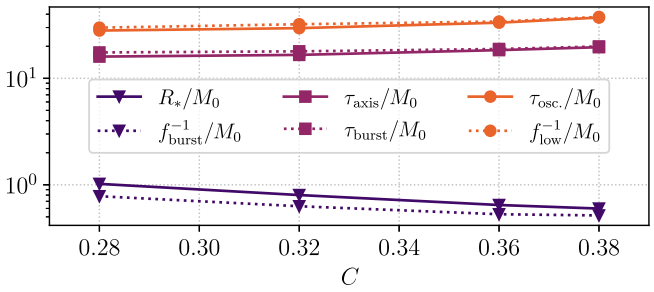

FIG. 4. The timescales associated with the gravitational waveforms emitted after the prompt emissions for all four binaries. We show the secondary's size $R_* \approx M_0/(\eta C)$, the frequency $f_{\rm burst}$ of the first burst, the light crossing time $\tau_{\rm axis}$, the burst period $\tau_{\rm burst}$, the dominant remnant oscillation period $\tau_{\rm osc.}$, and the frequency $f_{\rm low}$ of the long-lived component.

$\ell = 2$ mode exhibits low-frequency oscillations between the high-frequency burst. Physically, this quadrupolar contribution originates from oscillation modes of the remnant star excited during the merger. In Fig. 4, we compare the fundamental frequency $f_{\rm low}$ of this component to the oscillation period $\tau_{\rm osc.}$ of the remnants (measured from postmerger oscillations of max $|\Phi|$), finding good agreement as a function of remnant compactness: $\tau_{\rm osc} \approx f^{-1}_{\rm low}$. The signal, $\tilde{\Psi}_4$, is dominated by the $n = 1$ harmonic of $f_{\rm low}$, where each harmonic has frequency $(n+1)f_{\rm low}$ (see also the Fourier transform in Fig. 3). Notice also that $f_{\rm low} \approx f^{\rm Kerr}_{\ell m=20}/2$. Roughly, the dominant frequency in the ℓth mode of this second GW component scales as $f^{\ell>2}_{\rm low} \sim \ell$. As can be seen in Fig. 3, this component is long-lived, with longer decay timescales than our simulations. The equally spaced frequency spectrum, the long-lived nature, together with the observation $f^{-1}_{\rm low} \approx 2\tau_{\rm burst}$, are indicative of trapped modes, which objects with stable light rings generally exhibit [101] (see also Refs. [13,102,103]). Lastly, we find no evidence that the amplitude of this long-lived component decreases with increasing compactness.

The amplitude of $\tilde{\Psi}_4$, however, should be interpreted with care. The observationally relevant strain h scales as $h(\omega) \sim \tilde{\Psi}_4(\omega)/\omega^2$ in the Fourier domain. Hence, high-frequency features are suppressed by a factor of $\sim\omega^{-2}$ compared to low-frequency components of $\tilde{\Psi}_4$. Therefore, and this must be emphasized, at the level of the strain the amplitude of the long-lived component is larger than the amplitude of the bursts for all $\ell \lesssim 6$ modes (and larger than the prompt response in all considered modes). In turn, the amplitude of the bursts is larger than the prompt response for $\ell \gtrsim 4$ only.

Lastly, the total GW energy $E_<(t)$ radiated through a sphere of radius of $r_{\rm extr.}$ up to time t for the $C = 0.38$ binary

is $E_<(t_0+\tau_{\rm burst})/M_0 \approx 6\times10^{-6}$ and $E_<(t_0+5\tau_{\rm burst})/M_0 = 6\times10^{-5}$. The energy $E_<(t)$ still increases roughly linearly with rate $\dot{E}_< \approx 8\times10^{-7}$ at this time. In contrast, the total radiated energy of the head-on collision of a (nonspinning) binary black hole with the same mass-ratio is $\lim_{t\to\infty} E_<(t) = 2\times10^{-6}M_0$ [104]; this is consistent with the energy emission by the black hole–boson star merger considered in this work.

Discussion and conclusion—In this work, we performed the first nonlinear and self-consistent study of the ringdown of a black hole mimicker. We broadly confirm the appearance of features in the emitted gravitational waveform expected based on test-field approaches. However, we also found that the dynamics of the mimicker's internal degrees of freedom have large impact on the emitted GWs.

Although, the sequence of remnants, considered in this work, becomes increasingly more compact, there are no polar light spheres, and the primary's exterior is (by construction) not parametrically close to the Kerr exterior. Therefore, it is remarkable that the waveforms in Fig. 1 match at all, and in principle, any difference can be attributed to the differing exteriors. In analogy to the black hole case [104–107], the small compactness of the secondary, $C_* = 0.02$, likely has small impact on the prompt response of the remnant in low-ℓ modes.

GW echoes—features of the scattering of massless waves in black hole mimicker spacetimes neglecting any kind of backreaction—are expected to exhibit frequencies and decay rates of the order of the Kerr quasinormal modes at early times [18,24,48]. In this work, we identified two distinct frequency components of the waveform emitted after the prompt response. One of these is consistent with the quasinormal mode frequencies of a black hole of the same mass and spin, but long-lived, while the other is burstlike in nature, but with frequencies much higher than those quasinormal frequencies. Therefore, either component could ambiguously be labeled "the echoes." Since the bursts originate in perturbations of the mimicker's internal degrees of freedom and scale with the size of the secondary, test-field approaches are generally insufficient to capture this component [108]. Lastly, we find no evidence of a nonlinear instability in the binary constituents or remnants [1,109,110].

Acknowledgments—We would like to thank Niayesh Afshordi, Alejandro Cárdenas-Avendaño, Will East, Suvendu Giri, Luis Lehner, Elisa Maggio, and Frans Pretorius for many interesting discussions about aspects of this work. We especially thank Will East and Frans Pretorius for comments on an earlier version of this draft. The author is pleased to acknowledge that the work reported on in this Letter was substantially performed using the Princeton Research Computing resources at Princeton University which is a consortium of groups led by the Princeton Institute for Computational Science and Engineering (PICSciE) and Office of Information Technology's Research Computing. This work used Anvil at Purdue University through allocation PHY230198 from the Advanced Cyberinfrastructure Coordination Ecosystem: Services & Support (ACCESS) program [111], which is supported by National Science Foundation Grants No. 2138259, No. 2138286, No. 2138307, No. 2137603, and No. 2138296.

[1] V. Cardoso and P. Pani, Living Rev. Relativity **22**, 4 (2019).
[2] V. Cardoso, E. Franzin, and P. Pani, Phys. Rev. Lett. **116**, 171101 (2016); **117**, 089902(E) (2016).
[3] V. Cardoso, S. Hopper, C. F. B. Macedo, C. Palenzuela, and P. Pani, Phys. Rev. D **94**, 084031 (2016).
[4] V. Cardoso and P. Pani, Nat. Astron. **1**, 586 (2017).
[5] B. Holdom and J. Ren, Phys. Rev. D **95**, 084034 (2017).
[6] P. Bueno, P. A. Cano, F. Goelen, T. Hertog, and B. Vercnocke, Phys. Rev. D **97**, 024040 (2018).
[7] C. Barceló, R. Carballo-Rubio, and L. J. Garay, J. High Energy Phys. 05 (2017) 054.
[8] A. Urbano and H. Veermäe, J. Cosmol. Astropart. Phys. 04 (2019) 011.
[9] G. Raposo, P. Pani, M. Bezares, C. Palenzuela, and V. Cardoso, Phys. Rev. D **99**, 104072 (2019).
[10] P. Pani and V. Ferrari, Classical Quantum Gravity **35**, 15LT01 (2018).
[11] V. Cardoso, V. F. Foit, and M. Kleban, J. Cosmol. Astropart. Phys. 08 (2019) 006.
[12] N. Oshita and N. Afshordi, Phys. Rev. D **99**, 044002 (2019).
[13] Q. Wang, N. Oshita, and N. Afshordi, Phys. Rev. D **101**, 024031 (2020).
[14] N. Oshita, Q. Wang, and N. Afshordi, J. Cosmol. Astropart. Phys. 04 (2020) 016.
[15] E. Maggio, L. Buoninfante, A. Mazumdar, and P. Pani, Phys. Rev. D **102**, 064053 (2020).
[16] R. Dey, S. Chakraborty, and N. Afshordi, Phys. Rev. D **101**, 104014 (2020).
[17] T. Ikeda, M. Bianchi, D. Consoli, A. Grillo, J. F. Morales, P. Pani, and G. Raposo, Phys. Rev. D **104**, 066021 (2021).
[18] Z. Mark, A. Zimmerman, S. M. Du, and Y. Chen, Phys. Rev. D **96**, 084002 (2017).
[19] H. Nakano, N. Sago, H. Tagoshi, and T. Tanaka, Prog. Theor. Exp. Phys. **2017**, 071E01 (2017).
[20] Q. Wang and N. Afshordi, Phys. Rev. D **97**, 124044 (2018).
[21] C. P. Burgess, R. Plestid, and M. Rummel, J. High Energy Phys. 09 (2018) 113.
[22] M. R. Correia and V. Cardoso, Phys. Rev. D **97**, 084030 (2018).
[23] Luis Felipe Longo Micchi and C. Chirenti, Phys. Rev. D **101**, 084010 (2020).
[24] E. Maggio, A. Testa, S. Bhagwat, and P. Pani, Phys. Rev. D **100**, 064056 (2019).
[25] M. Srivastava and Y. Chen, Phys. Rev. D **104**, 104006 (2021).

[26] L. Annulli, V. Cardoso, and L. Gualtieri, Classical Quantum Gravity **39**, 105005 (2022).
[27] S. Xin, B. Chen, R. K. L. Lo, L. Sun, W.-B. Han, X. Zhong, M. Srivastava, S. Ma, Q. Wang, and Y. Chen, Phys. Rev. D **104**, 104005 (2021).
[28] S. Ma, Q. Wang, N. Deppe, F. Hébert, L. E. Kidder, J. Moxon, W. Throwe, N. L. Vu, M. A. Scheel, and Y. Chen, Phys. Rev. D **105**, 104007 (2022).
[29] A. Maselli, S. H. Völkel, and K. D. Kokkotas, Phys. Rev. D **96**, 064045 (2017).
[30] A. Testa and P. Pani, Phys. Rev. D **98**, 044018 (2018).
[31] K. W. Tsang, M. Rollier, A. Ghosh, A. Samajdar, M. Agathos, K. Chatziioannou, V. Cardoso, G. Khanna, and C. Van Den Broeck, Phys. Rev. D **98**, 024023 (2018).
[32] L. F. Longo Micchi, N. Afshordi, and C. Chirenti, Phys. Rev. D **103**, 044028 (2021).
[33] J. Abedi, H. Dykaar, and N. Afshordi, Phys. Rev. D **96**, 082004 (2017).
[34] G. Ashton, O. Birnholtz, M. Cabero, C. Capano, T. Dent, B. Krishnan, G. D. Meadors, A. B. Nielsen, A. Nitz, and J. Westerweck, arXiv:1612.05625.
[35] J. Westerweck, A. B. Nielsen, O. Fischer-Birnholtz, M. Cabero, C. Capano, T. Dent, B. Krishnan, G. Meadors, and A. H. Nitz, Phys. Rev. D **97**, 124037 (2018).
[36] R. S. Conklin, B. Holdom, and J. Ren, Phys. Rev. D **98**, 044021 (2018).
[37] A. B. Nielsen, C. D. Capano, O. Birnholtz, and J. Westerweck, Phys. Rev. D **99**, 104012 (2019).
[38] R. K. L. Lo, T. G. F. Li, and A. J. Weinstein, Phys. Rev. D **99**, 084052 (2019).
[39] K. W. Tsang, A. Ghosh, A. Samajdar, K. Chatziioannou, S. Mastrogiovanni, M. Agathos, and C. Van Den Broeck, Phys. Rev. D **101**, 064012 (2020).
[40] N. Uchikata, H. Nakano, T. Narikawa, N. Sago, H. Tagoshi, and T. Tanaka, Phys. Rev. D **100**, 062006 (2019).
[41] R. Abbott *et al.* (LIGO Scientific and Virgo Collaborations), Phys. Rev. D **103**, 122002 (2021).
[42] R. Abbott *et al.* (LIGO Scientific, Virgo, and KAGRA Collaborations), arXiv:2112.06861.
[43] N. Uchikata, T. Narikawa, H. Nakano, N. Sago, H. Tagoshi, and T. Tanaka, Phys. Rev. D **108**, 104040 (2023).
[44] A. Miani, C. Lazzaro, G. A. Prodi, S. Tiwari, M. Drago, E. Milotti, and G. Vedovato, Phys. Rev. D **108**, 064018 (2023).
[45] J. Abedi, N. Afshordi, N. Oshita, and Q. Wang, Universe **6**, 43 (2020).
[46] R. Carballo-Rubio, F. Di Filippo, S. Liberati, and M. Visser, Phys. Rev. D **98**, 124009 (2018).
[47] U. Danielsson, L. Lehner, and F. Pretorius, Phys. Rev. D **104**, 124011 (2021).
[48] V. Vellucci, E. Franzin, and S. Liberati, Phys. Rev. D **107**, 044027 (2023).
[49] C. Dailey, N. Afshordi, and E. Schnetter, Classical Quantum Gravity **40**, 195007 (2023).
[50] D. J. Kaup, Phys. Rev. **172**, 1331 (1968).
[51] R. Ruffini and S. Bonazzola, Phys. Rev. **187**, 1767 (1969).
[52] F. E. Schunck and E. W. Mielke, Classical Quantum Gravity **20**, R301 (2003).
[53] S. L. Liebling and C. Palenzuela, Living Rev. Relativity **26**, 1 (2023).
[54] R. Friedberg, T. D. Lee, and A. Sirlin, Phys. Rev. D **13**, 2739 (1976).
[55] C. Palenzuela, I. Olabarrieta, L. Lehner, and S. L. Liebling, Phys. Rev. D **75**, 064005 (2007).
[56] C. Palenzuela, L. Lehner, and S. L. Liebling, Phys. Rev. D **77**, 044036 (2008).
[57] C. Palenzuela, P. Pani, M. Bezares, V. Cardoso, L. Lehner, and S. Liebling, Phys. Rev. D **96**, 104058 (2017).
[58] M. Bezares, C. Palenzuela, and C. Bona, Phys. Rev. D **95**, 124005 (2017).
[59] T. Helfer, U. Sperhake, R. Croft, M. Radia, B.-X. Ge, and E. A. Lim, Classical Quantum Gravity **39**, 074001 (2022).
[60] M. Bezares and C. Palenzuela, Classical Quantum Gravity **35**, 234002 (2018).
[61] M. Bezares, M. Bošković, S. Liebling, C. Palenzuela, P. Pani, and E. Barausse, Phys. Rev. D **105**, 064067 (2022).
[62] T. Evstafyeva, U. Sperhake, T. Helfer, R. Croft, M. Radia, B.-X. Ge, and E. A. Lim, Classical Quantum Gravity **40**, 085009 (2023).
[63] N. Siemonsen and W. E. East, Phys. Rev. D **107**, 124018 (2023).
[64] N. Siemonsen and W. E. East, Phys. Rev. D **108**, 124015 (2023).
[65] N. Sanchis-Gual, C. Herdeiro, J. A. Font, E. Radu, and F. Di Giovanni, Phys. Rev. D **99**, 024017 (2019).
[66] N. Sanchis-Gual, J. C. Bustillo, C. Herdeiro, E. Radu, J. A. Font, S. H. W. Leong, and A. Torres-Forné, Phys. Rev. D **106**, 124011 (2022).
[67] L. Pierini and L. Gualtieri, Phys. Rev. D **106**, 104009 (2022).
[68] F. E. Schunck and E. W. Mielke, Rotating boson stars, in *Relativity and Scientific Computing: Computer Algebra, Numerics, Visualization*, edited by F. W. Hehl, R. A. Puntigam, and H. Ruder (Springer, Berlin, Heidelberg, 1996), pp. 138–151.
[69] M. S. Volkov and E. Wohnert, Phys. Rev. D **66**, 085003 (2002).
[70] B. Kleihaus, J. Kunz, and M. List, Phys. Rev. D **72**, 064002 (2005).
[71] N. Siemonsen and W. E. East, Phys. Rev. D **103**, 044022 (2021).
[72] See Supplemental Material at http://link.aps.org/supplemental/10.1103/PhysRevLett.133.031401 for details on the boson star parameter space and numerical techniques, which includes Refs. [73–96].
[73] R. A. Isaacson, Phys. Rev. **166**, 1263 (1968).
[74] S. L. Pitz and J. Schaffner-Bielich, Phys. Rev. D **108**, 103043 (2023).
[75] G. D. Birkhoff and R. E. Langer, *Relativity and Modern Physics* (Harvard University Press, Cambridge, 1923).
[76] J. T. Jebsen, Ark. Mat. Astron. Fys. **15** (1921).
[77] F. Pretorius, Classical Quantum Gravity **22**, 425 (2005).
[78] W. E. East, F. M. Ramazanoglu, and F. Pretorius, Phys. Rev. D **86**, 104053 (2012).
[79] C. Gundlach, J. M. Martin-Garcia, G. Calabrese, and I. Hinder, Classical Quantum Gravity **22**, 3767 (2005).
[80] W. E. East, F. Pretorius, and B. C. Stephens, Phys. Rev. D **85**, 124010 (2012).

[81] M. Alcubierre, S. Brandt, B. Bruegmann, D. Holz, E. Seidel, R. Takahashi, and J. Thornburg, Int. J. Mod. Phys. D **10**, 273 (2001).
[82] M. W. Choptuik and F. Pretorius, Phys. Rev. Lett. **104**, 111101 (2010).
[83] L. Lindblom and B. Szilagyi, Phys. Rev. D **80**, 084019 (2009).
[84] R. Friedberg, T. D. Lee, and Y. Pang, Phys. Rev. D **35**, 3658 (1987).
[85] T. D. Lee, Phys. Rev. D **35**, 3637 (1987).
[86] T. D. Lee and Y. Pang, Phys. Rep. **221**, 251 (1992).
[87] Y. S. Kobayashi, M. Kasai, and T. Futamase, Phys. Rev. D **50**, 7721 (1994).
[88] C. W. Misner, K. S. Thorne, and J. A. Wheeler, Gravitation Cosmol. (1973).
[89] P. V. P. Cunha, J. Grover, C. Herdeiro, E. Radu, H. Runarsson, and A. Wittig, Phys. Rev. D **94**, 104023 (2016).
[90] P. V. P. Cunha, E. Berti, and C. A. R. Herdeiro, Phys. Rev. Lett. **119**, 251102 (2017).
[91] C. J. Goebel, Astrophys. J. **172**, L95 (1972).
[92] L. G. Collodel and D. D. Doneva, Phys. Rev. D **106**, 084057 (2022).
[93] M. Bošković and E. Barausse, J. Cosmol. Astropart. Phys. 02 (2022) 032.
[94] S. Yoshida, Y. Eriguchi, and T. Futamase, Phys. Rev. D **50**, 6235 (1994).
[95] C. F. B. Macedo, V. Cardoso, L. C. B. Crispino, and P. Pani, Phys. Rev. D **93**, 064053 (2016).
[96] C. Vásquez Flores, A. Parisi, C.-S. Chen, and G. Lugones, J. Cosmol. Astropart. Phys. 06 (2019) 051.
[97] N. Sanchis-Gual, F. Di Giovanni, M. Zilhão, C. Herdeiro, P. Cerdá-Durán, J. A. Font, and E. Radu, Phys. Rev. Lett. **123**, 221101 (2019).
[98] Note, while the $C = 0.38$ star exhibits no strictly bound polar null geodesics (i.e., a light sphere), there are "quasi"-bound such geodesics as detailed in the Supplemental Material.
[99] E. Berti, V. Cardoso, and A. O. Starinets, Classical Quantum Gravity **26**, 163001 (2009).
[100] E. Berti, V. Cardoso, and C. M. Will, Phys. Rev. D **73**, 064030 (2006).
[101] K. D. Kokkotas and B. G. Schmidt, Living Rev. Relativity **2**, 2 (1999).
[102] C. F. B. Macedo, P. Pani, V. Cardoso, and L. C. B. Crispino, Phys. Rev. D **88**, 064046 (2013).
[103] P. Heidmann, N. Speeney, E. Berti, and I. Bah, Phys. Rev. D **108**, 024021 (2023).
[104] U. Sperhake, V. Cardoso, C. D. Ott, E. Schnetter, and H. Witek, Phys. Rev. D **84**, 084038 (2011).
[105] M. Davis, R. Ruffini, W. H. Press, and R. H. Price, Phys. Rev. Lett. **27**, 1466 (1971).
[106] W. E. East and F. Pretorius, Phys. Rev. D **87**, 101502(R) (2013).
[107] W. E. East, Astrophys. J. **795**, 135 (2014).
[108] In fact, naively applying these perturbative methods, one would *not* expect the waveforms to exhibit echoes, because the boson star's light-crossing time is comparable to Kerr quasinormal mode decay timescales.
[109] J. Keir, Classical Quantum Gravity **33**, 135009 (2016).
[110] P. V. P. Cunha, C. Herdeiro, E. Radu, and N. Sanchis-Gual, Phys. Rev. Lett. **130**, 061401 (2023).
[111] T. J. Boerner, S. Deems, T. R. Furlani, S. L. Knuth, and J. Towns, *Practice and Experience in Advanced Research Computing (PEARC '23)* (ACM, New York, 2023), 10.1145/3569951.3597559.